ACS Chemical Neuroscience

Research Article

pubs.acs.org/acschemicalneuroscience

An Azobenzene Photoswitch Sheds Light on Turn Nucleation in Amyloid-β Self-Assembly

Todd M. Doran,[†] Elizabeth A. Anderson,[†] Sarah E. Latchney,[‡] Lisa A. Opanashuk,[‡] and Bradley L. Nilsson*,[†]

[†]Department of Chemistry, University of Rochester, Rochester, New York 14627, United States

[‡]Department of Environmental Medicine, University of Rochester School of Medicine and Dentistry, Rochester, New York 14642, United States

Supporting Information

ABSTRACT: Amyloid-β (Aβ) self-assembly into cross-β amyloid fibrils is implicated in a causative role in Alzheimer's disease pathology. Uncertainties persist regarding the mechanisms of amyloid self-assembly and the role of metastable prefibrillar aggregates. Aβ fibrils feature a sheet-turn-sheet motif in the constituent β-strands; as such, turn nucleation has been proposed as a rate-limiting step in the self-assembly pathway. Herein, we report the use of an azobenzene β-hairpin mimetic to study the role turn nucleation plays on Aβ self-assembly. [3-(3-Aminomethyl)phenylazo]phenylacetic acid (AMPP) was incorporated into the putative turn region of Aβ42 to elicit temporal control over Aβ42 turn nucleation; it was hypothesized that self-assembly would be favored in the *cis*-AMPP conformation if β-hairpin formation occurs during Aβ self-assembly and that the *trans*-AMPP conformer would display attenuated fibrillization propensity. It was unexpectedly observed that the *trans*-AMPP Aβ42 conformer forms fibrillar constructs that are similar in almost all characteristics, including cytotoxicity, to wild-type Aβ42. Conversely, the *cis*-AMPP Aβ42 congeners formed nonfibrillar, amorphous aggregates that exhibited no cytotoxicity. Additionally, *cis-trans* photoisomerization resulted in rapid formation of native-like amyloid fibrils and *trans*−*cis* conversion in the fibril state reduced the population of native-like fibrils. Thus, temporal photocontrol over Aβ turn conformation provides significant insight into Aβ self-assembly. Specifically, Aβ mutants that adopt stable β-turns form aggregate structures that are unable to enter folding pathways leading to cross-β fibrils and cytotoxic prefibrillar intermediates.

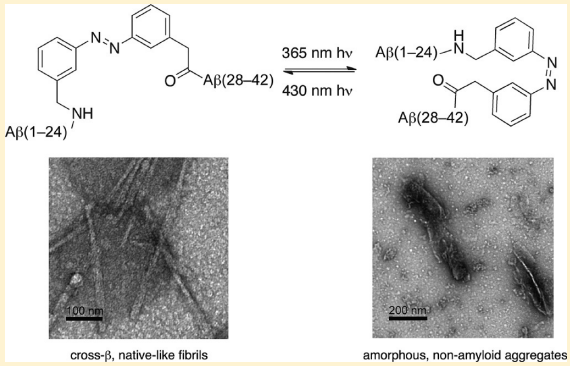

KEYWORDS: *Amyloid-β, turn nucleation, Alzheimer's disease, β-turn, amyloid fibrils, azobenzene photoswitch*

Amyloid-β (Aβ) is a 39−43 amino acid peptide that is the major constituent of the neuritic plaques that are hallmarks of Alzheimer's disease (AD).[1,2] Aβ is cleaved from the amyloid precursor protein (APP) and undergoes a series of self-association events that lead to the formation of oligomeric aggregates and, ultimately, cross-β fibrils.[3−7] Evidence suggests that soluble, prefibrillar oligomers, and not mature fibrils, are the toxic congeners in the AD brain.[8,9] Despite mounting evidence that implicates oligomers as the more cytotoxic congener of AD, Aβ oligomer structure−function studies have been impeded by the transitory nature of these species. This is due to the strong propensity for oligomers to self-associate into more thermodynamically stable cross-β fibrils.[10−12] It is therefore necessary to devise methods and conditions to control the folding pathway to gain insight into the structure−function activity of these species on AD pathology.[12]

The structure of Aβ fibrils and prefibrillar intermediates has been extensively studied.[13−18] Solid-state NMR studies and molecular dynamics simulations on Aβ40 indicate that fibrils are composed of a cross-β morphology that features a sheet-turn-sheet motif, with the turn region comprising residues 23−28.[15−17,19−21] Riek et al. have proposed a similar structure in Aβ42 fibrils, with a bend encompassed by residues 26 through 30.[22] NMR analysis of monomeric Aβ structures suggests that a bend region between residues 24−27 connects N-terminal and C-terminal helices under membrane-mimetic conditions.[23,24] Smith et al. have identified a turn in Aβ42 oligomers between residues 25 and 29, and a turn flanked by a D23/K28 salt bridge in the fibril structure.[12] Collectively, these data suggest that turn formation within early folding intermediates of Aβ may nucleate fibrillogenesis by facilitating α-helix → β-sheet oligomer → β-sheet fibril transitions.

Turn nucleation in the 24−30 region of Aβ has been proposed to be an early folding event in Aβ fibril nucleation.[25−27] Turn nucleation has been probed experimentally by restricting the turn region with a lactam heterocycle formed by the condensation of D23 and K28 into an amide

Received: November 25, 2011
Revised: January 9, 2012
Published: January 9, 2012

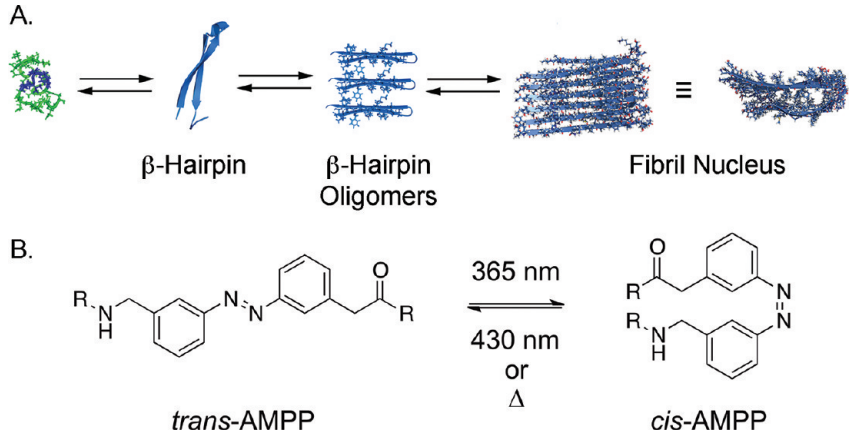

Figure 1. (A) Proposed Aβ fibrillization pathway depicting major folding events as nascent Aβ monomer self-associates into a fibril nucleus. (B) AMPP in the *trans* (left) and *cis* (right) conformations.

bond; enforcing the turn led to accelerated rates of self-assembly.[28] Recently, the structure of a β-hairpin conformer stabilized by an affibody ligand was reported; it was proposed that a similar hairpin structure may be an early intermediate during Aβ self-assembly.[26] Based on the hypothesis that β-hairpin formation is a rate-limiting step in Aβ fibril self-assembly, we sought a structural probe that would enable reversible temporal control of Aβ turn nucleation in order to perturb the equilibria of early structural conformers of Aβ that are relevant to self-assembly events. It was reasoned that this type of structural probe would provide significant insight into the possible role of turn nucleation in Aβ self-assembly and cytotoxicity.

Herein, we report the incorporation of a photoswitchable turn mimetic into the turn region of Aβ42 to elicit temporal control of turn nucleation. Azobenzene moieties have been used extensively to perturb the tertiary and quaternary structure of peptides.[29−38] We chose to use the azobenzene derivative [3-(3-aminomethyl)phenylazo]phenylacetic acid (AMPP) (Figure 1), which was developed specifically as a β-hairpin mimetic.[36−38] AMPP can be selectively photoisomerized into *cis* or *trans* conformations; the *cis* conformer has been shown to nucleate β-hairpin turns in the context of peptides.[35] We hypothesized that nucleating the turn in Aβ42 using the AMPP photoswitch would nucleate fibrillization. We conjectured that, in the *trans*-conformation, the turn region would lie in an extended conformation that precludes efficient self-assembly.

These hypotheses were explored by incorporation of AMPP into the 25−27 region of Aβ42 as either a two- or three-amino acid substitution. It was found that the self-assembly of AMPP-containing Aβ42 mutants was affected strongly by AMPP conformation. Unexpectedly, the *trans*-conformer readily assembled into fibrils that were indistinguishable from wild-type in nearly every aspect, including cytotoxicity. Conversely, *cis*-AMPP conformers assembled rapidly into aggregates that were dissimilar from typical Aβ42 cross-β amyloid. The *cis*-AMPP aggregates were sedimentable, but nonfibrillar and nontoxic under incubation conditions that favor either oligomer of fibril formation. Photoisomerization from *cis* → *trans* led to rapid fibrillogenesis from these nonfibril aggregates. This process could be reversed by *trans* → *cis* photoisomerization. Collectively, these results reveal that AMPP incorporated into the sequence of an amyloidogenic peptide can be used to reversibly manipulate early folding events during fibril nucleation. Aβ mutants that adopt stable β-turns form aggregate structures that are unable to enter folding pathways leading to cross-β fibrils and cytotoxic prefibrillar intermediates.

RESULTS AND DISCUSSION

Results. *Peptide Design and Rationale.* In order to assess the hypothesis that turn nucleation influences Aβ self-assembly, the azobenzene β-hairpin mimetic, AMPP, was incorporated into Aβ42 as a 2- or 3- amino acid substitution in the putative turn region (Table 1). In the context of peptides, *cis*-AMPP has been shown to be a type I′ β-hairpin backbone peptidomimetic, whereas *trans*-AMPP lies in a planar conformation (Figure 1B).[35] We hypothesized that, in the context of the Aβ42 peptide, the *trans*-azobenzene conformer would reduce self-assembly propensity (rate, thermodynamic stability of fibrils), while the *cis*-conformer would promote β-turn formation resulting in accelerated fibrillization. The position of the AMPP turn was chosen based on models proposed by Tycko and Smith, which place the turn between a D23/K28 salt bridge.[12,17,45] The Aβ42 peptide was chosen over Aβ40 because the time scale for Aβ42 fibril formation is considerably shorter than Aβ40, minimizing the likelihood of thermal *cis* → *trans* isomerization during the course of the experiment (the *trans* azobenzene conformation is thermodynamically favored). Fmoc-protected AMPP was prepared according to literature precedent[38] and the peptides shown in Table 1 (peptides **1**−**3**) were synthesized by standard Fmoc solid phase peptide synthesis (see Supporting Information for characterization and purification protocols).

Table 1. Aβ42 and Variant Peptides

peptide	variant	sequence
1	wild-type Aβ42	DAEFRHDSGYEVHHQKLVFFAEDVGSNK-GAIIGLMVGGVVIA
2	G25, S26, N27 → AMPP	DAEFRHDSGYEVHHQKLVFFAEDV[**AMPP**]-KGAIIGLMVGGVVIA
3	S26, N27 → AMPP	DAEFRHDSGYEVHHQKLVFFAEDVG[**AMPP**]K-GAIIGLMVGGVVIA

Conformational Switching between cis and trans Conformations. The extent of isomerization in AMPP-containing peptides was monitored using UV−vis absorbance spectroscopy. The AMPP chromophore exhibits a UV maximum at 330 nm when in the *trans* conformation that is reduced in the *cis* conformation coincident with the appearance

dx.doi.org/10.1021/cn2001188 | ACS Chem. Neurosci. 2012, 3, 211−220

of a weak maximum at 430 nm. Upon excitation with the appropriate wavelength of light, the AMPP photoswitch undergoes a conformational change; excitation at 430 nm induces the *trans* conformation, while excitation at 365 nm provides the *cis* conformation. Initial photoisomerization studies were conducted in DMSO in order to minimize complications from self-assembly. In the thermodynamically stable photostationary state, both **2** and **3** exist in the *trans* conformation (Figure 2). Following irradiation at 365 nm for

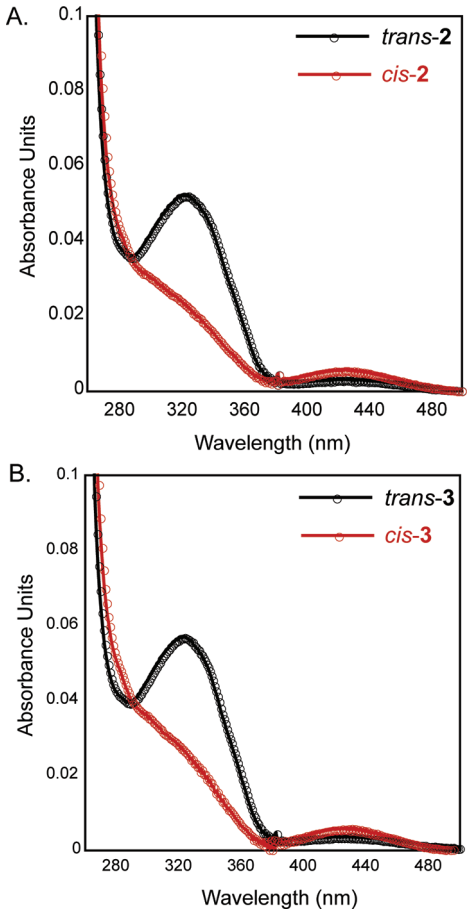

Figure 2. (A) Absorbance spectra for *trans*-**2** (black) and *cis*-**2** (red). (B) Absorbance spectra for *trans*-**3** (black) and *cis*-**3** (red). Spectra were obtained in DMSO.

30 min, efficient isomerization to the *cis* conformation occurs (Figure 2). Analytical HPLC was used to determine the extent of switching. Unfortunately, due to the high hydrophobicity of Aβ42, the peptide is difficult to resolve into narrow peaks by HPLC; as a result, the *cis* and *trans* conformers of the AMPP mutants **2** and **3** partially overlapped in HPLC spectra (Figures S1, S2). Based on these poorly resolved chromatograms, we were able to estimate that at least 65% of the total peptide concentration converts to *cis* upon *trans* → *cis* isomerization. The consequences of this incomplete conversion are discussed in following sections.

Kinetic Analysis of Aβ42 and AMPP Variant Self-Assembly. Fibril formation kinetics were monitored using a thioflavin T (ThT) fluorescence assay. ThT is a benzothiazole derivative that binds to amyloid cross-β fibrils.[46] Upon binding to fibrils, ThT undergoes a shift in its fluorescence emission spectrum, enabling observation of fibril formation in situ.[46] Self-assembly kinetics for freshly disaggregated peptide were monitored at 10 μM in phosphate buffered saline (pH 7.4).[39] The peptides were disaggregated, dissolved in DMSO, and photoisomerized to the desired conformation; these DMSO solutions were then diluted into phosphate buffered saline containing ThT and fibril growth was measured by fluorescence spectroscopy. Aβ self-assembly is nucleation-dependent as evidenced by an initial lag phase followed by exponential fibril growth.[47] ThT emission spectra curves were fit to eq 1 to obtain $t_{1/2}$ and k, where $t_{1/2}$ is the time required to reach one-half the maximum ThT emissions and k is the apparent rate constant. Lag time, the time required before the exponential growth phase, was calculated from these parameters using eq 2.

Contrary to our hypothesis, it was found that the *trans*-**2** and *trans*-**3** variants self-assembled similarly to wild-type Aβ42, whereas *cis*-**2** and *cis*-**3** failed to form amyloid-like fibrils that bound ThT (Figure 3). In fact, rate of self-assembly for both

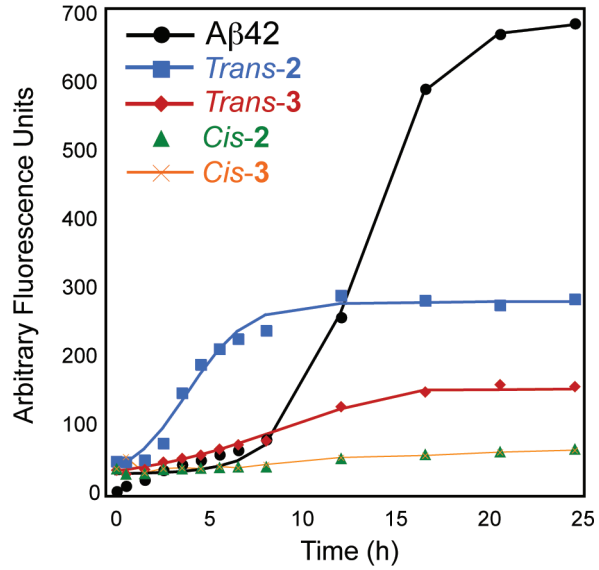

Figure 3. ThT fluorescence analysis of fibrillization kinetics for peptides **1**–**3**.

trans variants was moderately accelerated relative to wild-type Aβ42 (Table 2). The lag phases for self-assembly increased in

Table 2. Experimentally Derived Kinetic Parameters Obtained for the Self-Assembly of Aβ42 Variants

peptide		$t_{1/2}$ (h)	k (h^{-1})	lag time (h)
1	Aβ42	11 ± 2	0.3 ± 0.1	5 ± 2
2	*trans*-**2**	5 ± 1	1 ± 0.3	2 ± 1
2	*cis*-**2**	N/A	N/A	N/A
3	*trans*-**3**	7 ± 2	0.6 ± 0.2	2 ± 1
3	*cis*-**3**	N/A	N/A	N/A

the order *trans*-**2** ≈ *trans*-**3** > Aβ42. In addition to abbreviated lag times, the apparent rate of self-assembly (k) also increased in the order Aβ42 < *trans*-**2** ≈ *trans*-**3**. Differences in the magnitude of ThT fluorescence were observed between wild-type Aβ42 and the *trans*-**2** and -**3** variants. These differences could be due to differential binding of ThT based on variation in peptide conformations in the resulting fibrils. Alternatively, these differences could be attributed to quenching of ThT by the *trans*-AMPP chromophore. Experiments in which *trans*-

dx.doi.org/10.1021/cn2001188 | *ACS Chem. Neurosci.* 2012, 3, 211–220

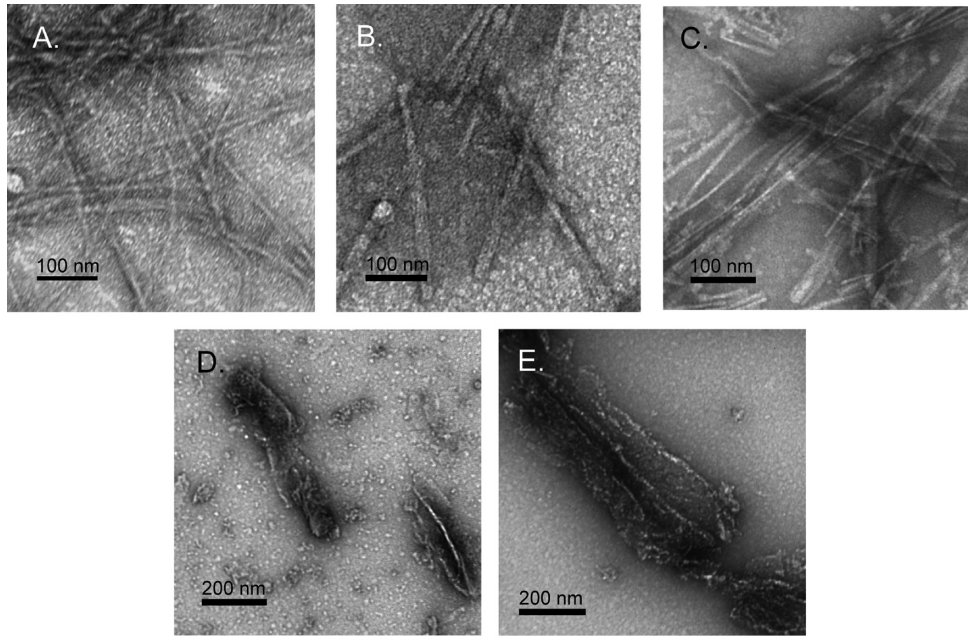

Figure 4. Transmission electron micrographs of fibrils derived from (A) Aβ42, (B) *trans*-**2**, (C) *trans*-**3**, (D) *cis*-**2**, and (E) *cis*-**3**.

AMPP is added to a mixture of mature fibrils and ThT resulted in a 10−15% decrease in ThT emission intensity; however, the proximity of ThT to the AMPP photoswitch in context of AMPP peptide variants may increase the magnitude of quenching observed.

Conversely, neither AMPP variant in the *cis* conformation exhibited significant ThT responses. In order to test whether the lack of ThT fluorescence in the *cis*-**1** and *cis*-**2** variants was due to ThT quenching by *cis*-AMPP, wild-type Aβ42 fibrils were spiked with increasing amounts of *cis*-**2** and *cis*-**3** and ThT fluorescence was measured. The degree of quenching observed in both cases was minor. Thus, these results suggest that the *cis*-AMPP variants fail to form cross-β fibrils.

The Effects of AMPP Turn Conformation on Cross-β fibril Morphology. Negative stain transmission electron microscopy (TEM) was used to image the aggregates derived from Aβ42 and each of the AMPP variants in both *trans* and *cis* conformations. Aβ42 formed striated fibrils with a diameter of 8.5 ± 1.8 nm (Figure 4A). *Trans*-**2** formed striated fibrils with diameters of 9.9 ± 2.2 nm, while *trans*-**3** formed fibrils of 7.0 ± 1 nm (Figure 4B,C). The filaments formed by Aβ42 resembled those derived from *trans*-**2** and *trans*-**3** in both size and appearance, which is an indication that they develop into similar cross-β fibrils. *Cis*-**2** and *cis*-**3** formed amorphous aggregates that did not resemble cross-β fibril morphology (Figure 4D,E). This explains the failure of these conformers to bind ThT.

Fibril secondary structure was further investigated using Fourier transform infrared spectroscopy (FT-IR). Peptide amide groups display a distinct amide I stretch at ∼1625 cm^{-1} in β-sheet secondary structures.[48] Aggregates derived from the each Aβ42 variants and conformers were collected by sedimentation and dehydrated. FT-IR analysis was performed on the dehydrated solids (Figure 5). Aβ42 exhibited an amide I stretch at 1628 cm^{-1}. A broad peak between 1650−1700 cm^{-1} was also observed, consistent with previous reports; this feature can be attributed to a combination of random coil structure from the disordered *N*-terminal region as well as sheet-turn-sheet turn structure.[49,50] *Trans*-**2** and *trans*-**3** fibrils displayed identical FT-IR amide I signatures with a stretch at ∼1630 cm^{-1} and a broad peak between 1650−1700 cm^{-1}. This data suggests that a similar sheet-turn-sheet motif is present in *trans*-**2** and *trans*-**3** fibrils as is observed in wild-type fibrils. Aggregates derived from *cis*-**2** and *cis*-**3** could also be collected by sedimentation; these aggregates displayed a strong stretch at 1680 cm^{-1} and only a very weak signal at 1628 cm^{-1}. This non-α/non-β IR signature is consistent with β-turn structure, but not with amyloid cross-β morphology.[48−50]

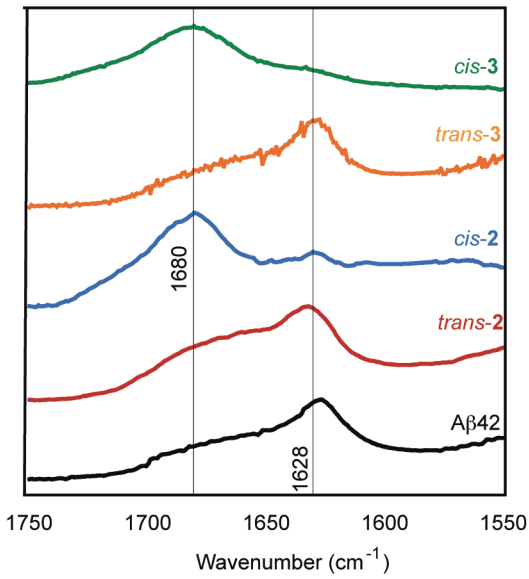

Figure 5. Normalized Fourier transform infrared spectra of aggregates derived from Aβ42 and AMPP variants thereof.

Congo Red Birefringence. Congo red birefringence was used to confirm the presence of cross-β fibrils in the *trans* variant samples and absence of cross-β amyloid in the *cis* samples.[51] Congo red binds amyloid fibrils and exhibits red/green birefringence under cross-polarized light, making it a

dx.doi.org/10.1021/cn2001188 | ACS Chem. Neurosci. 2012, 3, 211−220

useful diagnostic tool to detect amyloid.[51] Solutions of Aβ42 and each variant/conformation were allowed to self-assemble in phosphate-buffered saline at 10 μM concentrations. Aβ42 and the *trans*-**2** variant bound Congo red strongly as evidenced by light microscopy (Figure 6A,B) and digital micrographs of

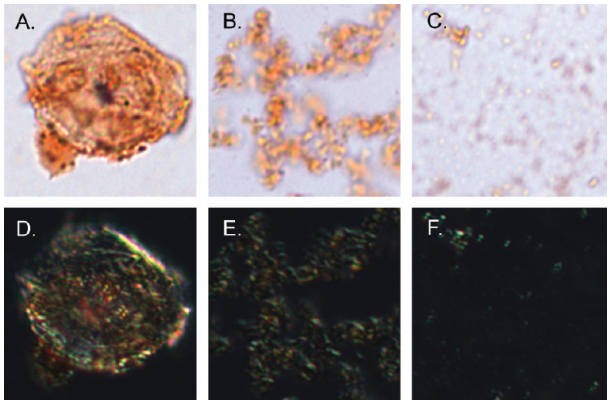

Figure 6. Congo red binding of fibrils derived from (A) Aβ42, (B) *trans*-**2**, and (C) *cis*-**2**. Congo red birefringence observed under cross-polarized light for (D) Aβ42, (E) *trans*-**2**, and (F) *cis*-**2**.

sedimented material (Figure S3). The *cis*-**2** conformer showed minimal binding of Congo red, indicated by the general absence of red in the light micrograph (Figure 6C) and absence of a red pellet after sedimentation (Figure S3). When viewed under cross-polarized light, strong green birefringence was observed for Aβ42 and the *trans* variant (Figure 6D,E), an indication of the presence of cross-β amyloid fibrils. *Cis*-**2**, however, displayed weak green birefringence, which is attributed to an absence of cross-β fibrils in this suspension. The small amount of Congo red binding and green birefringence observed in the *cis* samples are most likely due to a small amount of *trans*-**2** in the sample caused by incomplete photoisomerization. To ensure that Congo red anisotropy was observed, the absorbance spectrum of Congo red was recorded in the presence and absence of *cis*-**2** and *trans*-**2** (Figure S4). Upon binding fibrils, the change in anisotropy causes a red shift in the absorption spectrum of the dye to 540 nm; therefore, amyloid fibrils will thus exhibit a maximum absorbance at 540 nm when the sample spectrum is subtracted from the Congo red spectrum.[41,52] A large maximum at 540 nm was observed for *trans*-**2**, and only a minimal absorbance was observed for *cis*-**2** (Figure S4). This data suggests that Aβ42 and *trans*-**2** are competent to form amyloid fibrils with a cross-β architecture, whereas *cis*-**2** is not.

Sedimentation Analysis of Aβ42 and AMPP Variant Aggregates. Sedimentation analysis can be used to characterize the dynamic equilibrium between monomer and aggregate species in amyloid self-assembly processes.[39] Monomer and fibril (or other aggregates, including oligomer and other low or high order species) exist in equilibrium as expressed in the equation: $\text{fibril}_n + \text{monomer} \leftrightarrow \text{fibril}_{n+1}$. The critical concentration, C_r, is defined as the concentration of monomer present at equilibrium and represents the minimum amount of monomer that must be present to achieve self-assembly; C_r is characteristic of a given peptide sequence and is also dependent on self-assembly conditions.[39] C_r can be measured by sedimentation of the fibrils by centrifugation and quantification of the amount of monomer present in the supernatant using an HPLC calibration curve (see Methods).[39] The experimentally derived C_r is related to K_a for the addition of one monomer to fibril by eq 4 (Methods).[39] ΔG, a measure of fibril thermodynamic stability, can then be determined from K_a (Table 3), although ΔG values are only relevant for peptides

Table 3. Sedimentation Analysis for Aβ42 and AMPP Variant Self-Assembly

variant	C_r (μM)	ΔG (kcal/mol)	$\Delta\Delta G$ (kcal/mol)
Aβ42	2.4 ± 0.1	−7.7 ± 0.1	
trans-**2**	2.4 ± 1.0	−7.7 ± 0.2	0
cis-**2**	1.1 ± 0.3	NA	NA
trans-**3**	3.0 ± 0.8	−7.5 ± 0.1	+0.2 ± 0.1
cis-**3**	1.1 ± 0.3	NA	NA

that undergo similar self-assembly processes.[39] For example, in these studies, ΔG values that compare wild-type with each of the *trans* conformers are meaningful, whereas comparative ΔG values cannot be accurately attributed to the *cis* conformers that form unique aggregate types relative to wild-type and *trans* variants.

Wild-type Aβ42, *trans*-**2** and -**3**, and *cis*-**2** and -**3** each form sedimentable aggregates. The *trans* conformers exhibit similar C_r values to Aβ42 (Table 3). Assuming that the *trans* variants share a similar packing morphology to wild-type in the context of fibrils, it is possible to conclude that the thermodynamic stability of the fibrils derived from each of these species is similar (Table 3). While *cis*-**2** and *cis*-**3** do not bind ThT or Congo red, they do form aggregates that sediment with very low critical concentrations (Table 3). The relative thermodynamic stabilities of Aβ42 aggregates and the assemblies derived from the *cis*-variants cannot be accurately compared due to the different characteristics of the relative aggregates.

Effect of Turn Conformation on Cytotoxicity. The neurotoxicity of the turn variants was assessed. C17.2 neural precursor cells were exposed to Aβ42 and the respective AMPP variants in both *trans* and *cis* conformations as freshly disaggregated monomer or after incubation under conditions that favored the formation of oligomers (4 °C) or fibrils (37 °C) (Figure 7).[43,44] Cytotoxicity of the various aggregates was

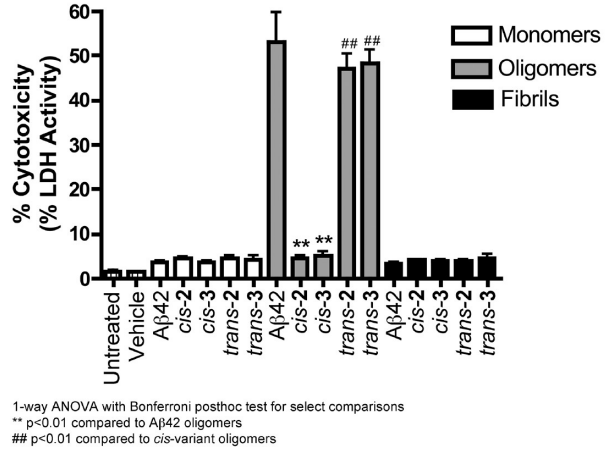

Figure 7. Cytotoxicity profiles of C17.2 neural progenitor cells after exposure to (1) freshly disaggregated Aβ42 variants (monomer); (2) Aβ42 variants grown under conditions that favor the formation of oligomers (oligomer); (3) aged Aβ42 variants grown under conditions that favor the formation of fibrils (fibril).

dx.doi.org/10.1021/cn2001188 | *ACS Chem. Neurosci.* 2012, 3, 211–220

determined by monitoring the activity of lactate dehydrogenase (LDH) that was released from the cells following membrane rupture as a result of cell death. As expected, freshly disaggregated monomer species of Aβ42 wild-type and each variant conformer were nontoxic.[43,44,53] Likewise, aggregates that were allowed to mature under conditions that favor fibril formation had low toxicity to cells under the assay conditions. Fibrils have previously been reported to be nontoxic and our results are consistent with this finding.[11] Aβ42 and the *trans*-**2** and *trans*-**3** variants that were incubated under conditions that have been shown to result in significant oligomer populations were highly toxic. Aβ42 oligomers exhibited toxicity values of ~53% and *trans*-**2** and *trans*-**3** oligomers had toxicity values of 47% and 48%, respectively, relative to detergent controls. Conversely, *cis*-**2** and *cis*-**3** incubated under oligomerization conditions were essentially nontoxic, with marginal toxicities of approximately 4% and 5%, respectively.

The toxicity of the conformational variants described herein is consistent with the self-assembly characteristics of each of these peptides. The high toxicity of the *trans* variants under conditions that favor the oligomer formation indicates that nonhairpin turns are present in toxic congeners, and that β-hairpin formation is not a prerequisite for this pathway. This is consistent with the work of Smith et al. who found that Aβ42 oligomers contain a nonhairpin turn. *Cis*-**2** and *cis*-**3** do not form cytotoxic species. This is not surprising given both morphological and kinetic data, which imply the *cis* conformers do not form aggregates with cross-β morphologies.

Photoconversion between Fibril and Nonfibril Aggregate States. The reversible photoconversion between fibril and nonfibril states was explored using peptide **2**. *Cis*-**2** was incubated at 10 μM concentration by dilution from DMSO into phosphate-buffered saline (pH 7.4) until sedimentation analysis indicated formation of aggregate; ThT binding was weak as described in the previous sections (Figure 8A). ThT was not present in the sample to avoid quenching of the fluorophore and to maintain consistent emission maxima throughout the experiment; ThT analysis was performed by dilution of aliquots of the assembly solution into ThT buffer.[54] After 24 h, when formation of aggregate was complete by sedimentation analysis, the sample irradiated at 365 nm for 3 h to affect *cis* → *trans* isomerization. After isomerization, ThT analysis indicated rapid, nearly immediate, formation of amyloid fibrils without an apparent lag phase. This lack of a lag phase was attributed to the long isomerization times employed, or the presence of small amounts of *trans*-**2** that had fibrillized during the initial 24 h, but remained nearly undetectable by ThT fluorescence. Alternatively, the preformation of aggregate in the *cis* state presumably enhances fibril formation by proximity effects.

The reversibility of fibril formation was assessed in *trans*-**2** fibrils after *trans* → *cis* photoisomerization. *Trans*-**2** was incubated until fibril formation was complete, as judged by having reached a maximum ThT emission plateau. The sample was irradiated at 365 nm for 3 h to affect a *trans* → *cis* isomerization. The sample was then monitored by ThT analysis for the presence of fibrils over time and compared with the original *trans*-**2** (Figure 8B). A decrease of ~60% ThT emission was observed following isomerization. This is consistent with an ~65% conversion observed in the analytical HPLC chromatograms. This data suggests that the fibrils were converted to a noncross-β morphology that is unable to bind ThT. Complete loss of ThT fluorescence did not occur due to incomplete photoisomerization of *cis* → *trans*. Therefore, the

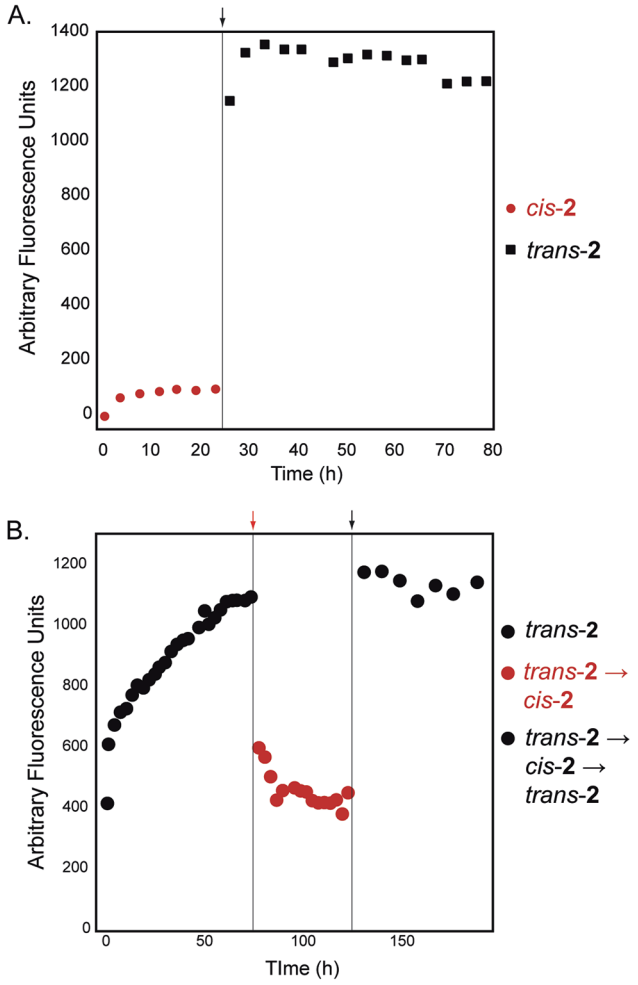

Figure 8. (A) Thioflavin T fluorescence analysis of *cis*-**2** converted to *trans*-**2** by irradiation with 434 nm light for 3 h (black arrow). Peptide samples were 10 μM in phosphate-buffered saline (pH 7.4). (B) Thioflavin T fluorescence analysis of *trans*-**2** converted to *cis*-**2** by irradiation with 365 nm light for 3 h (red arrow) followed by conversion of this sample to *trans*-**2** via irradiation at 434 nm light for 4 h (black arrow). Peptide samples were 10 μM in phosphate buffered saline (pH 7.4).

remaining ThT fluorescence is likely a result of residual, unconverted *trans*-**2** fibrils. The aggregates were characterized by FT-IR (Figure S5). *Cis*-**2** displayed an amide I stretch at ~1630 cm^{-1}, consistent with some retention of cross-β morphology, although the magnitude of this signal was significantly reduced from that exhibited by *trans*-**2**. This change in signal supports changes in aggregate structure upon photoconversion from *trans* → *cis*, although this conversion is clearly incomplete; the *cis* aggregates may also have unique structures relative to those that are formed by *cis*-**2** aggregation from the monomeric state. Irradiation of the *cis*-**2** sample at 434 nm for 4 h resulted in the complete restoration of ThT fluorescence correlating to reformation of fibrils upon photoisomerization from *cis* → *trans*. Thus, reversible conversion between fibril and nonfibril states can be affected by photoconversion in the assembled state. FT-IR of *trans*-**2** exhibited a stretching absorbance ~1630 cm^{-1}, consistent with the presence of β-sheet; however, the broad shoulder (as shown in Figure 5) disappeared (Figure S5). This data suggests that while aggregate structures can be switched from fibril to

dx.doi.org/10.1021/cn2001188 | *ACS Chem. Neurosci.* 2012, 3, 211–220

nonfibril states, the resulting photoisomerization of azobenzene is incomplete and that fibrils with different morphologies than those obtained originally may be obtained.

Discussion. Understanding the mechanism by which Aβ misfolds to form oligomers and fibrils is critical to understanding the correlation between self-assembly and AD pathology. Turn nucleation has been proposed as a rate-limiting step in Aβ fibrillogenesis.[55] It has specifically been suggested that β-hairpin intermediates form early during Aβ misfolding and that early aggregates feature β-hairpin oligomers that convert to the nonhairpin sheet-turn-sheet motif found in Aβ oligomers and fibrils.[26,27] Incorporation of an AMPP azobenzene photoswitch into the putative turn region of Aβ has provided insight into turn formation during Aβ fibrillogenesis.

It was found that Aβ variants containing *trans*-AMPP conformations formed fibrils similar to wild-type but that *cis*-AMPP conformers formed nonfibril aggregates that were nontoxic under all tested incubation conditions. The failure of the *cis*-AMPP variants to form fibrils may be due to the type of β-turn formed. The *cis*-AMPP photoswitch is a type I′ hairpin mimetic,[35] whereas that found in Aβ hairpin structures appears to be consistent with a type II′ turn[26] similar to turns formed by the D-ProGly nucleator introduced into the turn region by Chen and others.[56,57] In addition, Hilvert has found that unlike D-ProGly type II′ turns, the type I′ reverse turns generated by *cis*-AMPP are more mobile and the backbone of each proximal strand of the hairpin are flipped 180° reversing the hydrogen bonding pattern relative to type II′ turns.[38] Because hairpin stability is dictated by multiple factors, including hydrogen bonding, secondary structure propensities of residues in the strands, and side chain interactions, these differences could have a profound impact on the stability of the resultant conformations and impede transition to cross-β fibrils.[38] If *cis*-AMPP does form a type I′ turn in the context of peptide **2**, it may represent a non-native and highly stable β-hairpin conformation that precludes rotation into the nonhairpin turn found in Aβ oligomers and fibrils. Thus, *cis*-AMPP variants stabilize conformations that cannot enter folding pathways leading to cross-β fibrils. By bypassing these alternate conformations, the *trans*-AMPP moiety adopts a nonhairpin conformation conducive to fibril formation. However, without structural evidence that cis-AMPP forms a β-hairpin in the context of this peptide, the reason for its inability to progress to cross-β fibrils cannot be known and structural investigations of this peptide are currently underway.

The ability for *trans*-AMPP variants to form fibrils similar to wild-type Aβ is most likely due to the ability of these peptides to adopt the nonhairpin turn that is characteristic of Aβ fibrils according to NMR structures.[16,17,22] NMR analysis of AMPP-containing peptides by Dong et al. has shown that the *trans*-AMPP moiety in the context of a Trp zipper can form a nonhairpin turn.[35] This implies that β-hairpin formation is not a strict prerequisite for fibril nucleation and that formation of a nonhairpin turn is sufficient to nucleate fibrillogenesis. That *trans* AMPP facilitates the formation of nonhairpin turns in Aβ is consistent with the spectroscopic data obtained herein, which correlates to solid-state NMR models of Aβ40 proposed by Tycko and co-workers that predict a nonhairpin turn within the putative turn region.[16,17] Cytotoxicity of oligomers derived from the *trans* conformers was similar to wild-type oligomers, which is evidence that a β-hairpin turn is not required for cytotoxic oligomer formation. This data is also consistent with the work by Smith et al. who show that oligomers contain a nonhairpin bend.[12] The data reported herein is consistent with these models and clarifies the role of putative β-turn intermediates as a predecessor to a nonhairpin structure found in Aβ oligomers. While the existence of a hairpin intermediate cannot be conclusively ruled out on the basis of these studies, a putative β-hairpin intermediate is clearly not a strict requirement for the formation of Aβ oligomer and fibril structures.

■ CONCLUSION

The AMPP azobenzene photoswitch has been used as a tool to study the role of turn nucleation in Aβ self-assembly. To the best of our knowledge, this work represents the first time that a photoswitchable backbone mimetic has been incorporated into a pathogenic self-assembling peptide that undergoes complex folding mechanisms. The utility of AMPP-mediated conformational photoconversion to gain temporal control over the formation of Aβ oligomer and fibril structures has been demonstrated. These studies indicate that β-turn intermediates are not strictly required for Aβ fibril or cytotoxic oligomer formation. Studies are underway to investigate the potential of nontoxic congeners of Aβ based on *cis*-AMPP turn mimetics to perturb wild-type self-assembly and cytotoxicity.

■ METHODS

Peptide Synthesis and Purification. Solid-phase peptides synthesis was performed on a CEM Liberty microwave-equipped peptide synthesizer using Fmoc protection and HBTU/HOBt activation. Cleavage from the resin was obtained by suspension in TFA/TIS/H_2O (95:2.5:2.5, v/v/v) for 2 h followed by precipitation from diethyl ether. Purification was performed on a Shimadzu LC-AD HPLC with a reverse phase C18 column (19 mm × 250 mm; Waters, Milford, MA). A linear gradient of acetonitrile and water (0.1% TFA) was used as a mobile phase at 55 °C while monitoring eluent at absorbance at 215 nm. Analytical HPLC confirmed the purity of the peptide using a reverse phase C4 column (4.6 mm × 250 mm; Grace Vydac) (Figures S6−S10, Table S1). Peptide mass was confirmed by MADLI-TOF MS (Figures S11−S13, Table S2).

Peptide Disaggregation. The peptides were disaggregated using a modified Wetzel protocol.[39] In short, purified, lyophilized peptides were dissolved in TFA and sonicated at room temperature for ten minutes. The TFA was removed by evaporation using dry nitrogen. The resulting material was dissolved in HFIP and incubated at 37 °C. After 1 h, HFIP was evaporated using dry nitrogen and the peptide film was again dissolved in HFIP. Peptide concentration was determined from the HFIP solution by dilution into DMSO and HPLC analysis correlating the integrated peak area to a concentration curve calibrated by amino acid analysis (AIBiotech, Richmond, VA) (Figure S14−S15). The desired quantity of peptide was aliquoted into low-bind centrifuge tubes. HFIP was evaporated and the peptides were dried in vacuo overnight prior to dissolution in DMSO for self-assembly studies.

Azobenzene Peptide Photoisomerization. Peptide azobenzene photoisomerization was performed using a 500 W mercury lamp (Oriel). For *trans* → *cis* isomerization, freshly disaggregated peptide was dissolved in DMSO and transferred to a 0.1 cm quartz cuvette and irradiated for 30 min using a 365 nm cutoff filter. For *trans* → *cis* isomerization of fibrils in phosphate-buffered saline, the sample was irradiated at 365 nm for 3−5 h. C*is* → *trans* photoisomerization was affected by irradiation using a 434 nm cutoff filter for 4−5 h in phosphate-buffered saline (pH 7.4)

Kinetics of Fibril Self-Assembly. A thioflavin T (ThT) fluorescence assay was used to monitor self-assembly kinetics. Fluorescence experiments were carried out using a Tecan Infinite M1000 plate-reading fluorimeter using 96-well clear bottom non-binding microtiter plates (Greiner Bio-one) with excitation at 465 nm and emission monitored at 497 nm (10 nm bandwidth). Disaggregated

peptide was dissolved in DMSO (2 mM) and peptide concentration was confirmed by correlation of HPLC peak area to a standard concentration curve. DMSO stock solutions of peptide were diluted to 10 μM by addition of phosphate buffered saline (pH 7.4, 25 μM ThT). This solution was added to a 96-well microtiter plate and fluorescence was monitored at 25 °C. Fluorescence data was fit to the empirical sigmoid eq 1 where y_0 and y_{max} represent the initial and maximum fluorescence intensities, respectively; k is the apparent rate constant and $t_{1/2}$ is the time at which the fluorescence intensity reaches one-half the maximum value.[40] The lag time to self-assembly was calculated using eq 2.[40]

$$f(t) = y_0 + \frac{y_{max}}{1 + e^{-(t-t_{1/2})k}} \quad (1)$$

$$t_{lag} = t_{1/2} - \frac{2}{k} \quad (2)$$

Fibril Growth for Congo Red Birefringence, TEM, and FT-IR Analysis. Freshly disaggregated and dried peptides were dissolved in DMSO (2 mM) and peptide concentration was confirmed by correlation of HPLC integrated peak area to a standard concentration curve. The stock solution was diluted to 10 μM by addition of phosphate buffered saline (pH 7.4). Peptides were incubated at 25 °C for 3 days, and the resultant fibrils were used for Congo red birefringence, Fourier transform infrared spectroscopy (FT-IR), and negative-stain transmission electron microscopy (TEM).

Congo Red Staining and Birefringence Analysis. A 50 μM solution of Congo red stain (10 μL) was added to a 500 μL suspension of mature fibrils (10 μM), and the solution was incubated at 37 °C for 1 h. The resulting solution was centrifuged at 14 000g to sediment fibrils. The pellets were imaged with a digital camera.

Congo red staining was performed using a modified Nilsson protocol.[41] Briefly, a suspension of mature fibrils was centrifuged at 14 000g for 1 h to concentrate fibrils. After the supernatant was removed, the pellets were resuspended in a minimum volume of water. Two microliters of the suspension was applied to a glass microscope slide and allowed to air-dry in the dark. The Congo red staining solution was prepared by filtering a saturated solution of Congo red in 80% ethanol and saturated NaCl. Then 200 μL of this staining solution was applied to the slide and air-dried in the dark. Micrographs of Congo-red-stained specimens were obtained using a Nikon E600 light microscope (Nikon). Birefringence was observed by cross-polarizing the source light before and after the path of the sample at a 90° angle.

Equilibrium Sedimentation Assay. Disaggregated peptides were dissolved in DMSO and diluted by addition of the desired volume of phosphate buffered saline (pH 7.4). Solutions were incubated at 25 °C without agitation. An aliquot was removed and centrifuged (14 000g, 1 h, 4 °C) to remove fibrillar and oligomeric aggregates after 1 week and again 2 days later to ensure self-assembly had reached equilibrium. Monomeric peptide concentration was quantified by correlation to HPLC concentration curves. The monomer concentration at the end point defines the critical concentration, C_r, for the system. The C_r is indicative of the dynamic equilibrium between fibril and monomer at end point is represented by the expression: fibril$_n$ + monomer ↔ fibril$_{n+1}$.[39] At equilibrium, C_r is inversely related to the association constant, K_a, for the growth of the fibril by a single monomer unit,[39] as represented in eq 3.[39] C_r is related to K_a by eq 4.[39] ΔG values for each variant were determined using experimentally derived K_a values.

$$K_a = \frac{[\text{fibril}_{n+1}]}{[\text{fibril}_n][\text{monomer}]} \quad (3)$$

$$K_a = \frac{1}{C_r} \quad (4)$$

Negative Stain Transmission Electron Microscopy. Mature fibril suspensions (10 μL) were applied to 200 mesh, carbon-coated copper grids for 5 min. Excess fluid was removed by capillary action. Residual salts and buffer were washed with water (10 μL) for 10 s followed by removal by capillary action (repeated twice). The grids were stained with 5% uranyl acetate (10 μL) for 5 min and the excess staining solution was removed via capillary action. The stained grids were allowed to air-dry for at least 10 min prior to imaging. Electron microscope imaging was performed on a Hitachi 7650 transmission electron microscope in high contrast mode with an accelerating voltage of 80 kV. Fibril width was determined by performing at least 100 measurements on unique fibrils for each peptide using the program ImageJ (http://rsbweb.nih.gov/ij/).[42]

Fourier Transform Infrared Spectroscopy. Mature fibrils were prepared as described above and collected by centrifugation. The resulting concentrated fibrils were washed with D_2O, resuspended in a minimal amount of D_2O, frozen, and lyophilized. The lyophilized fibril was applied to the ATR stage of a Shimadzu FTIR-8400S spectrometer. IR spectra were obtained at a resolution of 2 cm^{-1}. Smoothing of the data and multipoint baseline correction was performed using IRSolution software.

Assessment of Variant Cytotoxicity. *C17.2 Cell Culture.* C17.2 neural precursor cells were maintained in Dulbecco's modified Eagle's medium (DMEM) media containing phenol red, 10% fetal bovine serum (FBS), 5% horse serum (HS), 4 mM L-Glutamine, 1 mM pyruvate and 1% penicillin/streptomycin in a humidified atmosphere of 5% CO_2 at 37 °C (herein referred to as feeding media). Media was changed every 2−3 days. Cells were grown in culture dishes to subconfluence before analysis.

Lactate Dehydrogenase Release Assay. Cytotoxicity was monitored for the various Aβ peptides by measuring the percentage of extracellular lactate dehydrogenase (LDH) leakage in the cell culture media. This assay is based on the oxidation of NADH by LDH and the conversion of pyruvate into lactate. The oxidation of NADH results in decreased absorbance at 340 nm and the rate of decrease in absorbance is directly proportional to LDH activity. C17.2 cells were seeded overnight in 96-well plates (BD Falcon) at a density of 3×10^3 cells per well in feeding media. Cells were then exposed for 24 h to vehicle (DMSO) or 1 μM Aβ peptides prepared as monomer, oligomer or fibrils. For treatment with monomeric Aβ, freshly disaggregated Aβ was dissolved in DMSO, sterilized by filtration, diluted to 1 μM in phenol-red-free, serum-free feeding media and immediately applied to cells. Oligomers were prepared as previously described.[43,44] Briefly, Aβ was incubated in phenol red-free DMEM media overnight at 4 °C (50 μM) and then diluted to 1 μM for application to cells. Fibrils were matured by incubating Aβ 100 μM for 1 week in phosphate buffered saline (pH 7.4). Fibrils were diluted to 1 μM in phenol-red-free, serum-free DMEM feeding media before addition to cells. 1% Triton X-100 was used as a positive control for total LDH release. Following the exposure period, 100 μL of the cell culture media was collected and centrifuged at 4000 rpm for 7 min at 4 °C. The enzyme activity of released LDH was measured by a diode array spectrophotometer utilizing UV−visible HP ChemStation software. LDH activity was calculated based on the extinction coefficient of NADH at 340 nm and pH 7.5 and expressed as the percentage of the total LDH released from the 1% Triton X-100 control.

Statistical Analyses. Three independent experiments were performed and the data are expressed as means ± standard error of the mean (SEM). Statistical analyses were performed with one-way repeated measures analysis of variance (ANOVA) (GraphPad Prism 4.0). For statistical significance, $p < 0.05$. Bonferroni post hoc tests were used to analyze significant ANOVAs.

■ ASSOCIATED CONTENT

Ⓢ Supporting Information

Peptide characterization data, peptide concentration curves, Congo red absorbance spectra, digital images, and FT-IR spectra. This material is available free of charge via the Internet at http://pubs.acs.org.

AUTHOR INFORMATION

Corresponding Author

*Telephone: (585) 276-3053. Fax: (585) 276-0205. E-mail: nilsson@chem.rochester.edu.

Author Contributions

B.L.N. conceived the project and designed experiments. T.M.D. designed experiments and synthesized AMPP; prepared all peptides; conducted photoisomerization experiments, kinetic assays, and sedimentation assays; performed TEM imaging; and conducted FT-IR, Congo red birefringence, and photo-induced switching assays. E.A.A., S.E.L., and L.A.O. planned and carried out cytotoxicity experiments. B.L.N. and T.M.D. co-wrote the manuscript.

Funding

This work was supported by a DuPont Young Professor Award to B.L.N. and by the Alzheimer's Association (NIRG-08-90797). Mass spectroscopy instrumentation was partially supported by grants from the U.S. National Science Foundation (CHE-0840410, CHE-0946653). L.A.O. and S.E.L. were supported by grants from the National Institutes of Health (T32ES07026 and P30ES01247).

Notes

The authors declare no competing financial interest.

ACKNOWLEDGMENTS

We gratefully acknowledge Karen Bentley of the University of Rochester Medical Center Electron Microscope Research Core for assistance with transmission electron microscopy experiments. We would like to thank Prof. Joseph Dinnocenzo for help with photoisomerization studies and helpful discussions. We also thank Prof. Christopher Welte for help with light microscopy and Congo red birefringence assays.

ABBREVIATIONS

Aβ, amyloid-β; AD, Alzheimer's disease; APP, amyloid precursor protein; AMPP, 3-(3-aminomethyl-phenylazo)-phenyl]-acetic acid; Fmoc, 9-fluorenylmethoxycarbonyl; HPLC, high-performance liquid chromatography; HBTU, *O*-benzotriazole-*N*,*N*,*N*′,*N*′-tetramethyl-uronium-hexafluorophosphate; HOBt, hydroxybenzotriazole; TFA, trifluoroacetic acid; TIS, triisopropyl silane; MALDI-TOF, matrix-assisted laser desorption ionization-time-of-flight mass spectrometry; HFIP, 2-hexafluoroisopropanol; ThT, thioflavin T; DMSO, dimethylsulfoxide; TEM, transmission electron microscopy; FT-IR, Fourier transform infrared; NMR, nuclear magnetic resonance

REFERENCES

(1) Haass, C., Schlossmacher, M. G., Hung, A. Y., Vigo-Pelfrey, C., Mellon, A., Ostaszewski, B. L., Lieberburg, I., Koo, E. H., Schenk, D., Teplow, D. B., and Selkoe, D. J. (1992) Amyloid β-peptide is produced by cultured cells during normal metabolism. *Nature 359*, 322−325.

(2) Seubert, P., Vigo-Pelfrey, C., Esch, F., Lee, M., Dovey, H., Davis, D., Sinha, S., Schlossmacher, M., Whaley, J., Swindlehurst, C., McCormack, R., Wolfert, R., Selkoe, D., Lieberburg, I., and Schenk, D. (1992) Isolation and quantification of soluble Alzheimer's β-peptide from biological fluids. *Nature 359*, 325−327.

(3) Hardy, J., and Selkoe, D. J. (2002) The Amyloid Hypothesis of Alzheimer's Disease: Progress and Problems on the Road to Therapeutics. *Science 297*, 353−356.

(4) Soto, C. (2003) Unfolding the role of protein misfolding in neurodegenerative diseases. *Nat. Rev. Neurosci. 4*, 49−60.

(5) Chiti, F., and Dobson, C. M. (2006) Protein Misfolding, Functional Amyloid, and Human Disease. *Annu. Rev. Biochem. 75*, 333−366.

(6) Jakob-Roetne, R., and Jacobsen, H. (2009) Alzheimer's Disease: From Pathology to Therapeutic Approaches. *Angew. Chem., Int. Ed. 48*, 3030−3059.

(7) Roychaudhuri, R., Yang, M., Hoshi, M. M., and Teplow, D. B. (2009) Amyloid β-Protein Assembly and Alzheimer Disease. *J. Biol. Chem. 284* (8), 4749−4753.

(8) Walsh, D. M., Klyubin, I., Fadeeva, J. V., Cullen, W. K., Anwyl, R., Wolfe, M. S., Rowan, M. J., and Selkoe, D. J. (2002) Naturally secreted oligomers of amyloid-β protein potently inhibit hippocampal long-term potentiation in vivo. *Nature 416*, 535−539.

(9) Walsh, D. M., and Selkoe, D. J. (2007) Aβ Oligomers — a decade of discovery. *J. Neurochem. 101*, 1172−1184.

(10) Bucciantini, M., Giannoni, E., Chiti, F., Baroni, F., Formigli, L., Zurdo, J., Taddei, N., Ramponi, G., Dobson, C. M., and Stefani, M. (2002) Inherent toxicity of aggregates implies a common mechanism for protein misfolding diseases. *Nature 416*, 507−511.

(11) Kayed, R., Head, E., Thompson, J. L., McIntire, T. M., Milton, S. C., Cotman, C. W., and Glabe, C. G. (2003) Common Structure of Soluble Amyloid Oligomers Implies Common Mechanism of Pathogenesis. *Science 300*, 486−489.

(12) Ahmed, M., Davis, J., Aucoin, D., Sato, T., Ahuja, S., Aimoto, S., Elliott, J. I., Sostrand, W. E. V., and Smith, S. O. (2010) Structural conversion of neurotoxic amyloid-β(1−42) oligomers to fibrils. *Nat. Struct. Mol. Biol. 17*, 561−567.

(13) Balbach, J. J., Petkova, A. T., Oyler, N. A., Antzutkin, O. N., Gordon, D. J., Meredith, S. C., and Tycko, R. (2002) Supramolecular Structure in Full-Length Alzheimer's β-Amyloid Fibrils: Evidence for a Parallel β-Sheet Organization from Solid-State Nuclear Magnetic Resonance. *Biophys. J. 83*, 1205−1216.

(14) Petkova, A. T., Ishii, Y., Balbach, J. J., Antzutkin, O. N., Leapman, R. D., Delaglio, F., and Tycko, R. (2002) A structural model for Alzheimer's β-amyloid fibrils based on experimental constraints from solid state NMR. *Proc. Natl. Acad. Sci. U.S.A. 99*, 16742−16747.

(15) Petkova, A. T., Leapman, R. D., Guo, Z., Yau, W.-M., Mattson, M. P., and Tycko, R. (2005) Self-Propagating, Molecular-Level Polymorphism in Alzheimer's β-Amyloid Fibrils. *Science 307*, 262−265.

(16) Petkova, A. T., Yau, W.-M., and Tycko, R. (2006) Experimental Constraints on Quaternary Structure in Alzheimer's β-Amyloid Fibrils. *Biochemistry 45*, 498−512.

(17) Paravastu, A. K., Leapman, R. D., Yau, W.-M., and Tycko, R. (2008) Molecular structural basis for polymorphism in Alzheimer's β-amyloid fibrils. *Proc. Natl. Acad. Sci. U.S.A. 105*, 18349−18354.

(18) Tycko, R. (2011) Solid-State NMR Studies of Amyloid Fibril Structure. *Annu. Rev. Phys. Chem. 62*, 279−299.

(19) Borreguero, J. M., Urbanc, B., Lazo, N. D., Buldyrev, S. V., Teplow, D. B., and Stanley, H. E. (2005) Folding events in the 21−30 region of amyloid β-protein (Aβ) studied *in silico*. *Proc. Natl. Acad. Sci. U.S.A. 102*, 6015−6020.

(20) Ma, B., and Nussinov, R. (2002) Stabilities and conformations of Alzheimer's β-amyloid peptide oligomers (Aβ_{16-22}, Aβ_{16-35}, and Aβ_{10-35}): Sequence effects. *Proc. Natl. Acad. Sci. U.S.A. 99*, 14125−14131.

(21) Miller, Y., Ma, B., and Nussinov, R. (2009) Polymorphism of Alzheimer's Aβ_{17-42} (p3) Oligomers: The Importance of the Turn Location and Its Conformation. *Biophys. J. 97*, 1168−1177.

(22) Lührs, T., Ritter, C., Adrian, M., Riek-Loher, D., Bohrmann, B., Döbeli, H., Schubert, D., and Riek, R. (2005) 3D structure of Alzheimer's amyloid-β(1−42) fibrils. *Proc. Natl. Acad. Sci. U.S.A. 102*, 17342−17347.

(23) Crescenzi, O., Tomaselli, S., Guerrini, R., Salvadori, S., D'Ursi, A. M., Temussi, P. A., and Picone, D. (2002) Solution structure of the Alzheimer amyloid β-peptide (1−42) in an apolar microenvironment. *Eur. J. Biochem. 269*, 5642−5648.

(24) Tomaselli, S., Esposito, V., Vangone, P., Nuland, N. A. J. v., Bonvin, A. M. J. J., Guerrini, R., Tancredi, T., Temussi, P. A., and Picone, D. (2006) The α-to-β Conformational Transition of

Alzheimer's Aβ-(1−42) Peptide in Aqueous Media is Reversible: A Step by Step Conformational Analysis Suggests the Location of β Conformation Seeding. *ChemBioChem 7*, 257−267.
(25) Lazo, N. D., Grant, M. A., Condron, M. C., Rigby, A. C., and Teplow, D. B. (2005) On the nucleation of amyloid β-protein monomer folding. *Protein Sci. 14*, 1581−1596.
(26) Hoyer, W., Grönwall, C., Jonsson, A., Ståhl, S., and Härd, T. (2008) Stabilization of a β-hairpin in monomeric Alzheimer's amyloid-β peptide inhibits amyloid formation. *Proc. Natl. Acad. Sci. U.S.A. 105*, 5099−5104.
(27) Sandberg, A., Luheshi, L. M., Söllvander, S., Barros, T. P. d, Macao, B., Knowles, T. P. J, Biverstål, H., Lendel, C., Ekholm-Petterson, F., Dubnovitsky, A., Lannfelt, L., Dobson, C. M., and Härd, T. (2010) Stabilization of neurotoxic Alzheimer amyloid-β oligomers by protein engineering. *Proc. Natl. Acad. Sci. U.S.A. 107*, 15595−15600.
(28) Sciaretta, K. L., Gordon, D. J., Petkova, A. T., Tycko, R., and Meredith, S. C. (2005) Aβ40-Lactam (D23/K28) Models a Conformation Highly Favorable for Nucleation of Amyloid. *Biochemistry 44*, 6003−6014.
(29) Beharry, A. A., and Woolley, G. A. (2011) Azobenzene photoswitches for biomolecules. *Chem. Soc. Rev 40*, 4422−4437.
(30) Woolley, G. A. (2005) Photocontrolling Peptide α-Helices. *Acc. Chem. Res. 38*, 486−493.
(31) Zhang, F., Zarrine-Afsar, A., Al-Abdul-Wahid, M. S., Prosser, R. S., Davidson, A. R., and Woolley, G. A. (2009) Structure-Based Approach to the Photocontrol fo Protein Folding. *J. Am. Chem. Soc. 131*, 2283−2289.
(32) Zhang, F., Timm, K. A., Arndt, K. M., and Woolley, G. A. (2010) Photocontrol of Coiled-Coil Proteins in Living Cells. *Angew. Chem., Int. Ed. 49*, 3943−3946.
(33) Deeg, A. A., Schrader, T. E., Kempter, S., Pfizer, J., Moroder, L., and Zinth, W. (2011) Light-Triggered Aggregation and Disassembly of Amyloid-Like Structures. *ChemPhysChem 12*, 559−562.
(34) Behrendt, R., Renner, C., Schenk, M., Wang, F., Wachtveitl, J., Oesterhelt, D., and Moroder, L. (1999) Photomodulation of the Conformation of Cyclic Peptides with Azobenzene Moieties in the Peptide Backbone. *Angew. Chem., Int. Ed. 38*, 2771−2774.
(35) Dong, S.-L., Loweneck, M., Schrader, T. E., Schreier, W. J., Moroder, L., and Renner, C. (2006) A Photocontrolled β-Hairpin Peptide. *Chem.—Eur. J. 12*, 1114−1120.
(36) Kräutler, V., Aemissegger, A., Hünenberger, P. H., Hilvert, D., Hansson, T., and Gunsteren, W. F. v. (2005) Use of Molecular Dynamics in the Design and Structure Determination of a Photo-inducible β-Hairpin. *J. Am. Chem. Soc. 127*, 4935−4942.
(37) Aemissegger, A., and Hilvert, D. (2007) Synthesis and application of an azobenzene amino acid as a light-switchable turn element in polypeptides. *Nat. Protoc. 2*, 161−167.
(38) Aemissegger, A., Kräutler, V., Gunsteren, W. F. v., and Hilvert, D. (2005) A Photoinducible β-Hairpin. *J. Am. Chem. Soc. 127*, 2929−2936.
(39) O'Nuallain, B., Thakur, A. K., Williams, A. D., Bhattacharyya, A. M., Chen, S., Thiagarajan, G., and Wetzel, R. (2006) Kinetics and Thermodynamics of Amyloid Assembly Using a High-Performance Liquid Chromatography-Based Sedimentation Assay. *Methods Enzymol. 413*, 34−74.
(40) Nielsen, L., Khurana, R., Coats, A., Frokjaer, S., Brange, J., Vyas, S., Uversky, V. N., and Fink, A. L. (2001) Effect of Environmental Factors on the Kinetics of Insulin Fibril Formation: Elucidation of the Molecular Mechanism. *Biochemistry 40*, 6036−6046.
(41) Nilsson, M. R. (2004) Techniques to study amyloid fibril formation in vitro. *Methods 34*, 151−160.
(42) Abramoff, M. D., Magelhaes, P. J., and Ram, S. J. (2004) Image Processing with ImageJ. *Biophotonics Int. 11*, 36−42.
(43) Dahlgren, K. N., Manelli, A. M., Stine, W. B., Baker, L. K., Krafft, G. A., and LaDu, M. J. (2002) Oligomeric and fibrillar species of amyloid-β peptides differentially affect neuronal viability. *J. Biol. Chem. 277*, 32046−32053.
(44) Stine, W. B., Dahlgren, K. N., Krafft, G. A., and LaDu, M. J. (2003) *In vitro* characterization of conditions for amyloid-β peptide oligomerization and fibrillogenesis. *J. Biol. Chem. 278*, 11612−11622.
(45) Luca, S., Yau, W.-M., Leapman, R., and Tycko, R. (2007) Peptide Conformation and Supramolecular Organization in Amylin Fibrils: Constraints from Solid-State NMR. *Biochemistry 46*, 13505−13522.
(46) LeVine, H. (1999) Quantification of β-Sheet Amyloid Fibril Structures with Thioflavin T. *Methods Enzymol. 309*, 274−284.
(47) Ferrone, F. (1999) Analysis of Protein Aggregation Kinetics. *Methods Enzymol. 309*, 256−274.
(48) Surewicz, W. K., Mantsch, H. H., and Chapman, D. (1993) Determination of Protein Secondary Structure by Fourier Transform Infrared Spectroscopy: A Critical Assessment. *Biochemistry 32*, 389−394.
(49) Szabó, Z., Klement, É., Jost, K., Zarándi, M., Soós, K., and Penke, B. (1999) An FT-IR Study of the β-Amyloid Conformation: Standardization of Aggregation Grade. *Biochem. Biophys. Res. Commun. 265*, 297−300.
(50) Chu, H.-L., and Lin, C.-Y. (2001) Temperature-induced conformational changes in amyloid β(1−40) peptide investigated by simultaneous FT-IR microspectroscopy with thermal system. *Biophys. Chem. 89*, 173−180.
(51) Nilsson, M. R., and Raleigh, D. P. (1999) Analysis of Amylin Cleavage Products Provides New Insights into the Amyloidogenic Region of Human Amylin. *J. Mol. Biol. 294*, 1375−1385.
(52) Klunk, W. E., Pettegrew, J. W., and Abraham, D. J. (1989) Two Simple Methods for Quantifying Low-affinity Dye-Substrate Binding. *J. Histochem. Cytochem. 37*, 1293−1297.
(53) Walsh, D. M., Townsend, M., Podlisny, M. B., Shankar, G. M., Fadeeva, J. V., Agnaf, O. E., Harley, D. M., and Selkoe, D. J. (2005) Certain Inhibitors of Synthetic Amyloid β-Peptide (Aβ) Fibrillogenesis Block Oligomerization of Natural Aβ and Thereby Rescue Long-Term Potentiation. *J. Neurosci. 25*, 2455−2462.
(54) O'Nuallain, B., Shivaprasad, S., Kheterpal, I., and Wetzel, R. (2005) Thermodynamics of Aβ(1−40) Amyloid Fibril Formation. *Biochemistry 44*, 12709−12718.
(55) Sciarretta, K. L., Gordon, D. J., Petkova, A. T., Tycko, R., and Meredith, S. C. (2005) Aβ40-Lactam (D23/K28) Models a Conformation Highly Favorable for Nucleation of Amyloid. *Biochemistry 44*, 6003−6014.
(56) Chang, E. S.-H., Liao, T.-Y., Lim, T.-S., Fann, W., and Chen, R. P.-Y. (2009) A New Amyloid-Like β-Aggregate with Amyloid Characteristics, Except Fibril Morphology. *J. Mol. Biol. 385*, 1257−1265.
(57) Haque, T. S., and Gellman, S. H. (1997) Insights on β-Hairpin Stability in Aqueous Solution from Peptides with Enforced Type I′ and Type II′ β-Turns. *J. Am. Chem. Soc. 119*, 2303−2304.